

Approaches to MRI Gating Using Multiple Sensors

Russell J. Iannuzzelli, Patrick N. Morgan, Bernard E. Kluga, and Michelle M. Rockwell

High-resolution images of the heart and coronary arteries produced by magnetic resonance imaging (MRI) typically require acquisition over multiple heart cycles. The goal of the work reported here was to develop an improved method of imaging coronary arteries using MRI that would minimize image artifacts caused by motion. We obtained information from a variety of sensors, including some that had never before been applied to MRI. This article gives a detailed description of our efforts to meet the stated goal. (Keywords: Cardiac gating, MRI, MRI gating, Sensors, Telemetry.)

INTRODUCTION

High-quality images of the heart and coronary arteries obtained by magnetic resonance imaging (MRI) are adversely affected by motion. In order to minimize the resulting image artifacts, gating to the heart and respiratory cycle is required. Typically, the heart cycle is monitored by an electrocardiograph (EKG), which measures changes in electrical potential occurring during the heartbeat, and the respiratory cycle is monitored using a pressure transducer (“bellows”) affixed around the abdomen.

In February 1997, APL began a collaborative effort with EPIX Medical, Inc., and the Laboratory of Cardiac Energetics of the National Heart, Lung, and Blood Institute (NHLBI, NIH) to develop an improved method of imaging coronary arteries using MRI. Specifically, APL was tasked to:

- Develop a computer hardware system that would correlate sensor data with MRI navigator data

- Develop suitable adaptive pattern recognition or correlation software algorithms
- Investigate and select a set of sensors that would produce the best correlation results
- Assist in volunteer or patient studies involving the use of the system at the NHLBI Laboratory of Cardiac Energetics

Our approach was to obtain information from a variety of sensors, including some that had never before been applied to MRI, in hopes of improving the cardiac and respiratory gating. Specifically, we used or evaluated 12 different sensors. In this article we present results from an EKG, a bellows, a single-channel Doppler radar, and an accelerometer. We also initially examined an M-mode ultrasound probe, in-phase (I) and quadrature-phase (Q) Doppler radar, an electric impedance measurement sensor, and a video field monitor, all of which showed promise but were not completely investigated.

We considered laser vibrometers, acoustophones, and piezoelectric devices as well, but these were ruled out because of high cost or speculated poor performance within a harsh acoustic and electromagnetic imaging environment.

Of the sensors used, we graded performance based on a correlation of the data with MRI navigator data aimed at the diaphragm. An MRI navigator is a specific type of scan that is not intended to produce an image. Rather, it is primarily used to identify interface position within a patient. It is a one-dimensional scan that is similar to an M-mode-type scan in ultrasound. Later in this article we present several snapshots of the MRI navigator data which clearly show the interface position moving. Ideally, the navigators would be aimed at the coronary arteries, but we were unable to obtain reliable results using the three-dimensional navigator pulse sequence developed by General Electric (GE). This article describes in detail our accomplishment of the tasks listed above.

SYSTEM DEVELOPMENT

Our Data Acquisition System interfaces with an MRI scanner to collect navigator data and with the sensors' electronics to collect sensor data. All of the software and much of the electronics were developed by APL.

We designed the Data Acquisition System with two primary functions in mind. First, it had to collect data from both the single-channel MRI scanner coil and from the various sensors simultaneously. This capability would allow us to analyze the data offline for possible correlations and patterns among the various sensors and the navigator MRI data. Second, the system had to be able to process the sensors in real time so that a better gating algorithm, if developed, could be implemented with the same base system, with a possible extension in the form of an added processor board. (Although such a gating algorithm was not used directly in the EPIX project, in a prototype aimed at producing real-time imaging, the identical hardware was successfully used with the addition of a processor board.)

Figure 1 is a block diagram of the Data Acquisition System used in the EPIX project. The MRI scanner is shown at the bottom; the receiver coil is attached to the patient. Initially, the system was interfaced to a GE Signa series scanner outfitted with four-channel analog fast receivers. About midway through the project, the Laboratory of Cardiac Energetics acquired an upgrade to an LX Model GE scanner. The only significant change due to the upgrade was to the center frequency of the demodulated echoes, which increased from 2.5 to 2.625 MHz.

The heavy dotted line in Fig. 1 represents a divider between the Magnet Room and the Scanner Electronics

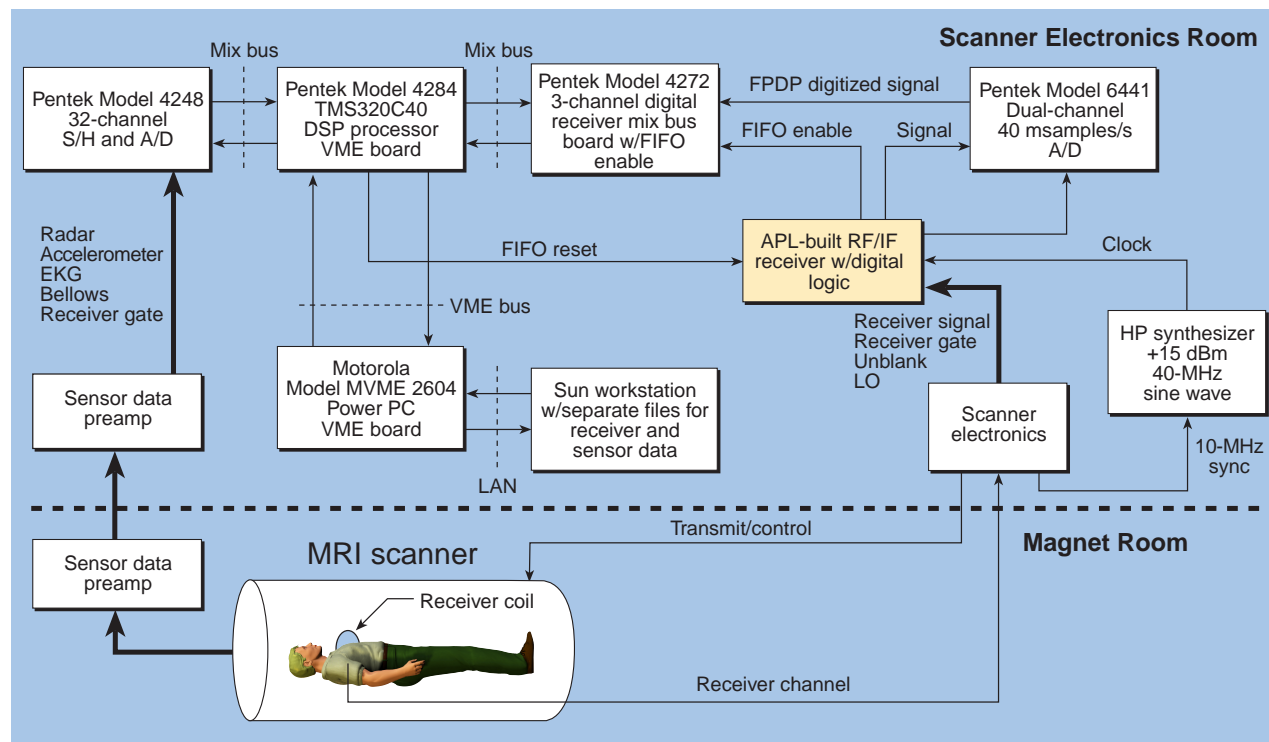


Figure 1. Block diagram of the Data Acquisition System. (S/H = sample and hold, A/D = analog-to-digital converter, DSP = Digital Signal Processor, FIFO = first-in/first-out, FPDP = front panel data port, LO = local oscillator, LAN = local area network.)

Room. All signals passing between these rooms go through the patch panel. The five signals from the scanner necessary to collect MRI navigator data are the surface coil signal, the echo gate signal, the unblank signal, the local oscillator (LO) signal, and the 10-MHz time-base reference signal. The time base is used to reference the HP synthesizer, which generates the 40-MHz sine wave. This synthesized sine wave signal is used to clock the digital logic in the analog receiver and the high-speed analog/digital (A/D) converter. The other four signals from the scanner go to the APL-built RF/IF analog demodulation box, which is functionally broken down in Fig. 2. Here, the MRI scanner is shown at the top. The signal off the receiver coil/preamp is sent through a bandpass filter to reduce out-of-band noise. It is then sent through a switch that passes the echo outside the unblank interval. This switch is necessary so that the bleed-through from the MR RF transmitter does not saturate or harm any of the components to follow. The signal is then amplified and mixed with the LO from the scanner. By using the LO from the scanner, the signal after mixing will always be positioned at 2.625 MHz, regardless of the actual transmit frequency. This is because the LO and the transmit are generated from the same set of direct digital synthesizers (DDS) within the MRI scanner electronics. The mixing is followed by a variable attenuator, low-pass filter, and amplifier. These components reject out-of-band frequencies and match the gain necessary at the A/D converter. The other elements in the RF/IF analog demodulation box are a splitter/amplifier path for the master clock and the digital logic that converts the sine wave clock into a TTL signal and buffers and latches the first-in/first-out (FIFO) control signals.

The outputs of the RF/IF analog demodulation box are the clock signal split, which goes to clock the

A/D, the demodulated and amplified coil signal, which is input into the A/D, and the FIFO enable control logic. The A/D output is used as the input to a digital receiver. Functionally, the digital receiver comprises a set of DDS used to generate a sine/cosine pair for I/Q mixing. After the mixing, which is a true multiply, I and Q are filtered with a combination of linear-phase filters. The output is then a complex echo, centered at DC, with an appropriate bandwidth selected by a filter/decimate parameter. The FIFO enable and reset logic were added to support a means of collecting data on the digital receiver board only when an echo gate was received. Engineers at Pentek modified the Model 4272 digital receiver mix board to include a FIFO enable/reset BNC connector on the front panel. Thus, the echo gate from the scanner turns on the FIFO, enabling it to collect output data. After these output data are transferred to the C40 processor board, the C40 processor puts out a pulse on the front panel to reset the digital receiver FIFO. In addition to controlling the data acquisition interval, the C40 routes data from the digital receiver to a file on a workstation. It also routes data from the A/D converter that are used to digitize the slow data sensor signals to a separate file on the workstation. In Fig. 1, this is shown as the Pentek Model 4248 32-channel simultaneously sampling A/D mix board. The mix bus is the local bus used for data input/output on the Pentek Model 4284 C40 processor board.

PREAMPLIFICATION

The sensor data are sent through two different preamp boxes, one in the Magnet Room and one in the Scanner Electronics Room. Separate preamp boxes were required to amplify the signals and filter 60 Hz and gradient noise on the signals. To obtain precise time stamping between the scanner data file and the sensor data file, the echo window gate was sampled with the sensor data set. This also allowed sensor data to be collected when the scanner was on and off. We will expand upon this feature in a later section.

The dual-preamp configuration shown in Fig. 1 was necessary to stabilize the signals in the Magnet Room, and then to perform notch filtering and general low-pass filtering in the Scanner Electronics Room. Figure 3 is a block diagram of the processing used in the preamp boxes. The radar had a voltage regulator and preamp circuit built into the cylindrical container. The preamp circuits only applied to the single-channel radar and the accelerometer. The EKG and the bellows used preexisting preamps built into the GE scanner. Some of the plots of data, shown later in the article, still exhibited gradient noise bleeding on the sensor signals. We determined that the cabling in the Magnet Room would need to be modified and possibly replaced with a fiber-optic set of communications channels.

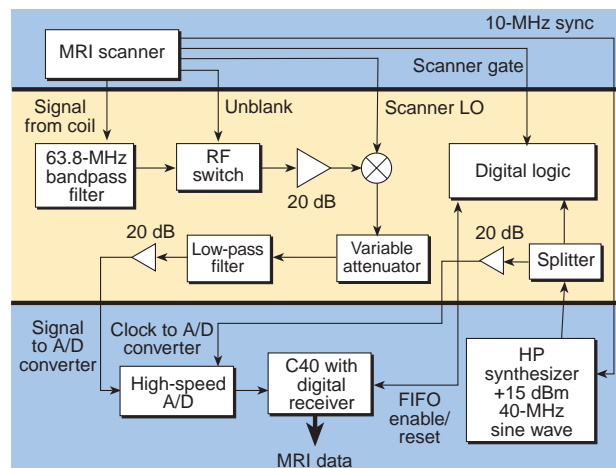


Figure 2. Expanded view of the APL-built RF/IF receiver with digital logic shown in Fig. 1.

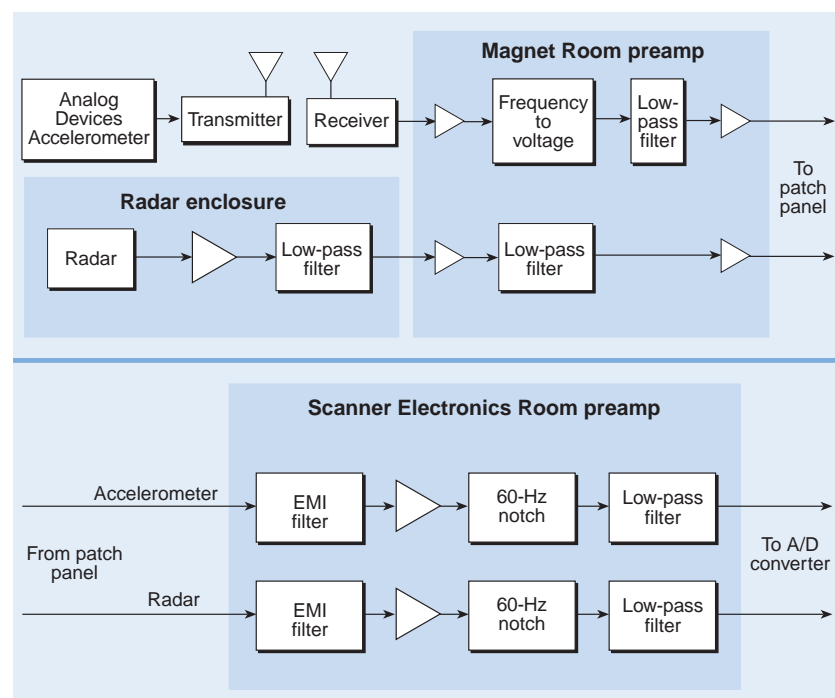


Figure 3. Block diagram of preamps used for radar and accelerometer.

SENSORS

We developed two new sensors to measure physiological data for the purpose of MRI gating. We also acquired data from existing MRI sensors (e.g., the bellows and EKG).

Radar

The first APL-developed sensor was a compact, low-cost K-band radar (Kustom Signals, Inc., Lenexa, KS), similar to those used in police speed monitors. To minimize RF interference to and from the MRI scanner, the radar was mounted in an aluminum enclosure along with APL-built circuitry for power regulation, preamplification, and offset trimming. This sensor has two major advantages: it can be used remotely from the patient and has high sensitivity to motion. Its principal disadvantage is poor specificity, which may be overcome with the use of MRI-compatible copper waveguide.

The radar signal contains information from objects moving along the direction of the radar beam. These objects produce an offset in the frequency f of the signal known as a Doppler shift. For example, an object moving at a velocity v produces a Doppler shift given by¹

$$\Delta f = 2v/\lambda, \quad (1)$$

where λ is the radar wavelength. For the K-band radar, $f = 35.5$ GHz, so $\lambda = c/f = 0.85$ cm. Hence, a slow-

moving object such as the chest wall, with a velocity of 5 cm/s, produces a Doppler shift $\Delta f = 12$ Hz. This Doppler shift is detectable using standard Fourier analysis with at least 83 ms of data.

The depth of penetration of the radar into human tissue can be approximated with the formula²

$$\delta = 1/\sqrt{\pi f \mu \sigma}, \quad (2)$$

where $\mu = 4\pi \times 10^{-7}$ H/m is the permeability of tissue, and σ is the electrical conductivity. At $f = 35.5$ GHz, $\sigma \approx 0.9$ S/m (Ref. 3), so $\sigma \approx 3$ mm. Hence, the radar signal will not penetrate much farther than the surface of the skin, which should be sufficient to detect respiratory motion. Although minimal information from the heart would be obtained directly, some information may be contained in the signal through compression of tissue

caused by heart motion or blood flow.

Figure 4 is a photograph of the radar. A laser level is attached to the aluminum enclosure to assist in aiming the device. A plot of the sensitivity of the radar with angle is shown in Fig. 5. The 3-dB beamwidth is about 8° . When mounted 5 m from the patient, the radar would illuminate a circular region of $10 \tan(4^\circ) = 70$ cm in diameter perpendicular to the beam. Since the radar is obliquely positioned relative to the patient inside the magnet bore, the actual region is somewhat larger.

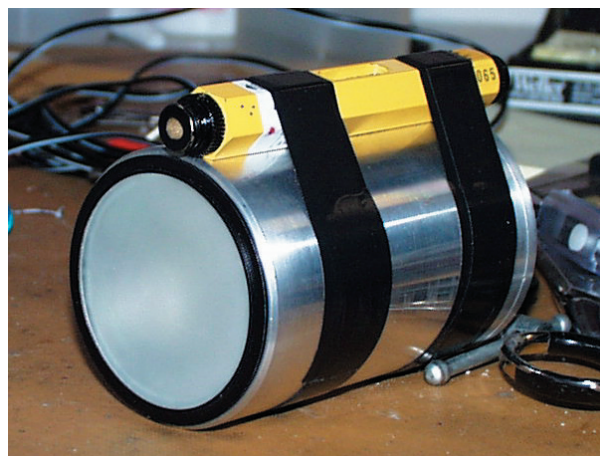


Figure 4. The radar sensor.

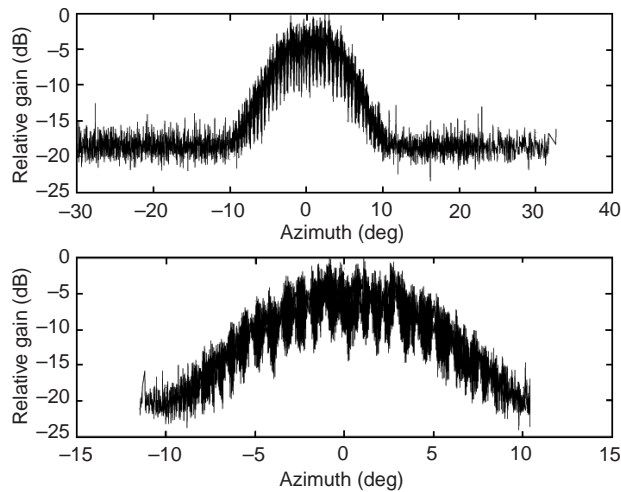


Figure 5. Radar azimuth data (operating frequency = 35.4848 GHz with 0° cutting angle).

Accelerometer with IR Wireless Telemetry

We also developed a sensor using a micromachined accelerometer (Analog Devices, Norwood, MA, ADXL05) mounted on a single monolithic integrated circuit. Rather than directly measuring chest wall acceleration, the device acts as a tilt sensor by measuring inclination of the chest or stomach relative to the Earth's gravitational field. To make the device wireless, we added an IR transmitter. Both devices, along with APL-built circuitry and MRI-compatible batteries, were mounted in an RF-shielded enclosure to prevent interference from the RF coils on the MRI scanner. One advantage of using this sensor is its high specificity, since the small size enables it to be placed anywhere on the patient to obtain localized measurements of tilt with high sensitivity. The principal disadvantage is corruption of the signal by the MRI gradient coils, which can be minimized by careful circuit design. A photograph of the accelerometer and IR transmitter is shown in Fig. 6.

Since the device was packaged in a metal can that was extremely magnetic, we asked the Electronic Services Group of APL's Technical Services Department to remove the cans from 10 devices and repackage them using nonmagnetic ceramics. The device and ceramic package were mounted on a small multilayer printed circuit board containing surface-mount components.

A circuit schematic is shown in Fig. 7. The device is powered by MRI-compatible lithium (Li) batteries (Ultralife Batteries, Inc., Newark, NJ) regulated to 5 V. The standard IR link used in television remote controls and other devices relies on a digital stream of IR pulses synchronized to a 38-kHz repetition rate. To improve the signal-to-noise ratio, most standard IR receivers have a built-in bandpass filter at 38 kHz. Since the

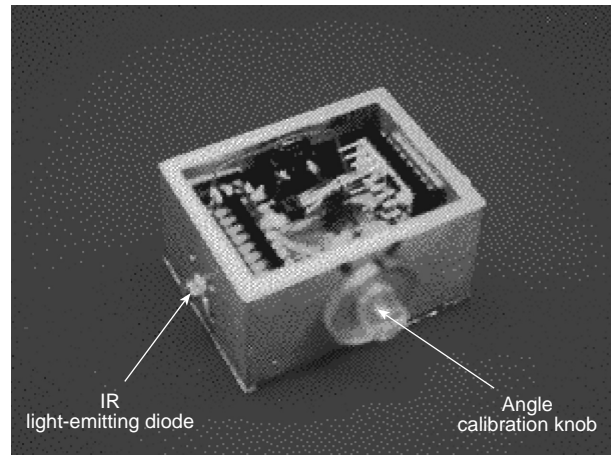


Figure 6. Accelerometer sensor and IR transmitter. The enclosure is about 5 cm wide \times 3.8 cm tall \times 3.8 cm deep. A plastic on/off switch is mounted on the back of the enclosure.

signal from the accelerometer is an analog voltage, we developed a frequency modulation technique involving two voltage-controlled oscillators (VCOs). The first VCO outputs a TTL signal from 0.7 to 1.7 kHz that is linearly proportional to the accelerometer voltage. That output drives a second VCO, which pulses the IR light-emitting diodes at a repetition rate of 36 to 41 kHz. Hence, at the receiver, a square wave is generated whose frequency varies from 0.7 to 1.7 kHz linearly with the accelerometer voltage. At the receiver, the FM square wave is carried by a nonmagnetic triaxial cable out of the Scanner Electronics Room into the APL-built circuit that converts frequency to voltage, the output of which is fed into the sensor A/D board. Figure 8 is a block diagram of the modulation techniques used in the IR and RF wireless approaches.

Video

We also considered directly digitizing a video signal of the patient's thorax. The patient would wear a tight-fitting black shirt with white stripes that would track respiratory or gross patient motion. One advantage of using this sensor is the ability to track motion noninvasively with good resolution in two spatial dimensions. The third spatial dimension along the camera axis could be inferred from magnification or distortion of the patterns. The sensor's principal disadvantage is its inability to track motion on patients who require a blanket.

Data obtained from a volunteer dressed as specified outside the magnet are shown in Fig. 9. The data sampling rate was 2.5 MHz, corresponding to 159 points per line of video data. The standard video format is 525 lines per interlaced image at 30 Hz. The stripes appeared as spikes in the video field (Fig. 9, left) and as white lines in the image (Fig. 9 right). The square dips

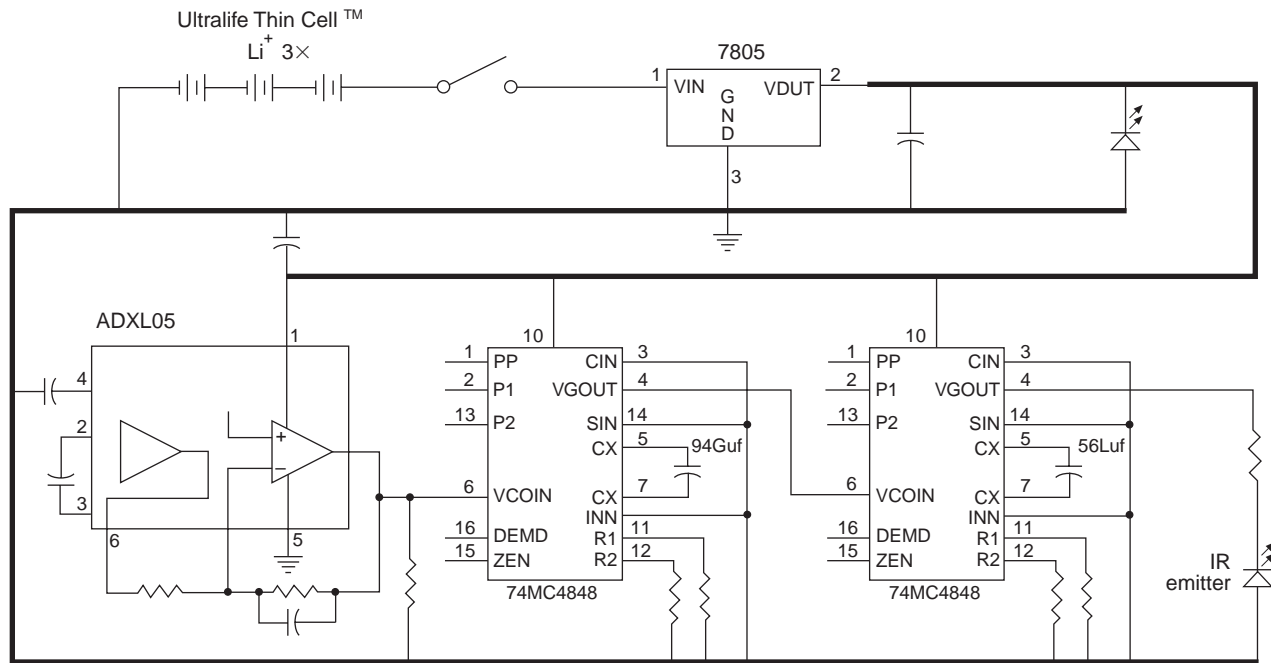


Figure 7. Circuit schematic of the accelerometer and IR transmitter. The ADXL05 was repackaged by APL into a nonmagnetic die.

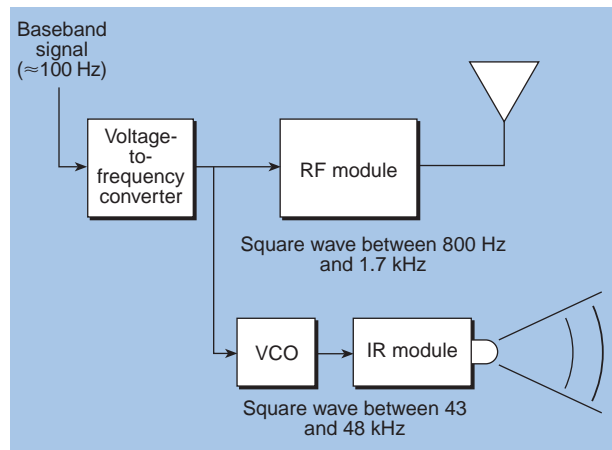


Figure 8. Wireless modulation techniques.

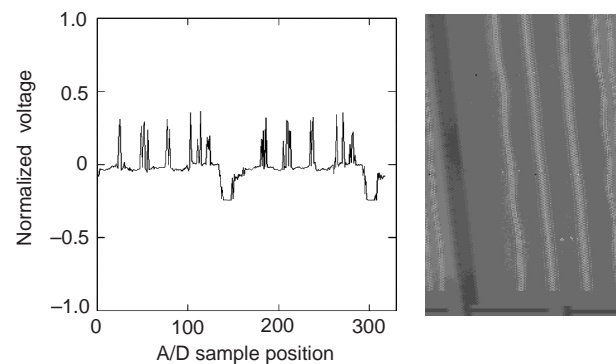


Figure 9. Video signal and corresponding image.

in the signal are the horizontal sync pulses. The carrier burst that follows the sync pulses is undersampled, but the video data are adequately sampled. The contrast-to-noise ratio of the stripes is about 12, and the spatial resolution is about 2×2 mm.

RF Telemetry

APL also developed an RF wireless system for the accelerometer. Two different transmit/receive modules were tried, the Linx Technologies HP series (900 MHz) and the LC series (434 MHz). The basic accelerometer with IR wireless telemetry device was duplicated and

modified to use either the HP or LC transmit module, which offered 50 kbps and 5 kbps modulation rates, respectively. The HP uses a frequency shift keying-type communications scheme and should typically yield a more robust communications approach than the LC on/off keying communications scheme. However, when placed near or in the main magnet, the HP series did not operate properly, perhaps owing to corruption of the oscillator. The LC series *did* continue to operate even in the magnet, but reception was so degraded that the receiver box had to be placed at the edge of the magnet bore. In both cases, accelerometer operation and modulation were identical to the wireless IR

approach, with the exception of bypassing the last modulation stage and feeding a sampled signal square wave from 0.7 to 1.7 kHz into the data pin on the two different transmitter modules. We investigated both spiral antennas and loop antennas on the transmitter. The results of these investigations are very promising and indicate that a robust RF wireless system for both EKG and inclination could be developed and used within the main magnet.

RESULTS

We verified operation of the Data Acquisition System and sensors using a moving table experiment as shown in Fig. 10. MRI navigator data were acquired from a ball phantom resting on the moving table and synchronized to an EKG signal generated outside the magnet. The bellows was attached between the moving table and a stable anchor point. The accelerometer was placed on the phantom. Data sampled from the MRI scanner and sensors included the radar, EKG, bellows, accelerometer, and MRI gate signal. A plot of the sensor data is shown in Fig. 11. The bellows data indicate the position of the table. When the table moves, there is an obvious Doppler frequency signal from the radar. Since the accelerometer does not tilt much when the table moves, the signal is approximately constant. When the MRI scanner is on, as indicated by the presence of the gate pulses, data from the radar and accelerometer are corrupted somewhat.

A plot of the navigator data from the same experiment is shown in Fig. 12. The data correspond to the first four gate pulses shown in Fig. 11. As the table moves, the edge of the ball moves to the edge of the frequency spectrum. The noise level at the edge is approximately -72 dB. Within the field of view, however, it is substantially higher, approximately -30 dB, due to loading of the receiver coil by the phantom.

To determine the accuracy of predicting heart position using the sensor data, we performed numerous correlations on data obtained from normal volunteers. The edge of the MRI navigator data provides an estimate of the diaphragm location. Since the heart rides on the diaphragm, the data also estimate the heart position, although the

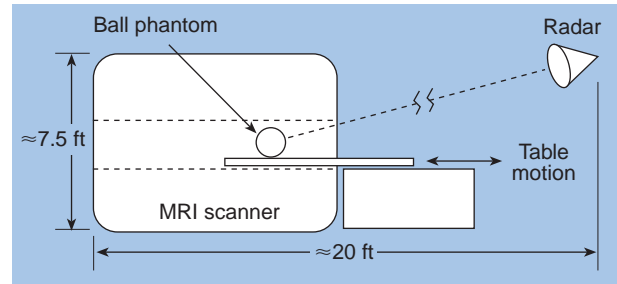


Figure 10. Sketch of the moving table experiment.

actual motion of the heart is more complicated. Future studies could point the navigator to the edge of the heart to obtain a better estimate of heart dynamics.

Bellows

A plot of the correlation between the stomach bellows and navigator position for 2 min of data is shown in Fig. 13. The tight clustering around a line indicates a repeatable linear correlation. Similar data were obtained from all volunteers. Hence, the stomach bellows provided an accurate estimate of diaphragm position, at least during the initial stages of the MRI examination. However, we noticed that in some volunteers this correlation was reduced as the scan progressed. In those volunteers, a bellows placed on the chest correlated more accurately with diaphragm position.

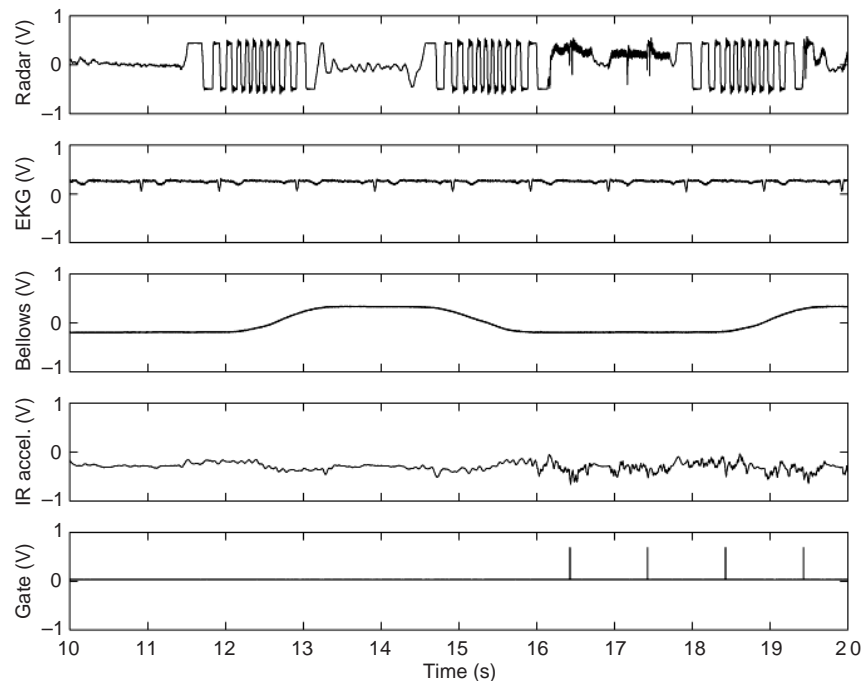


Figure 11. Sensor data.

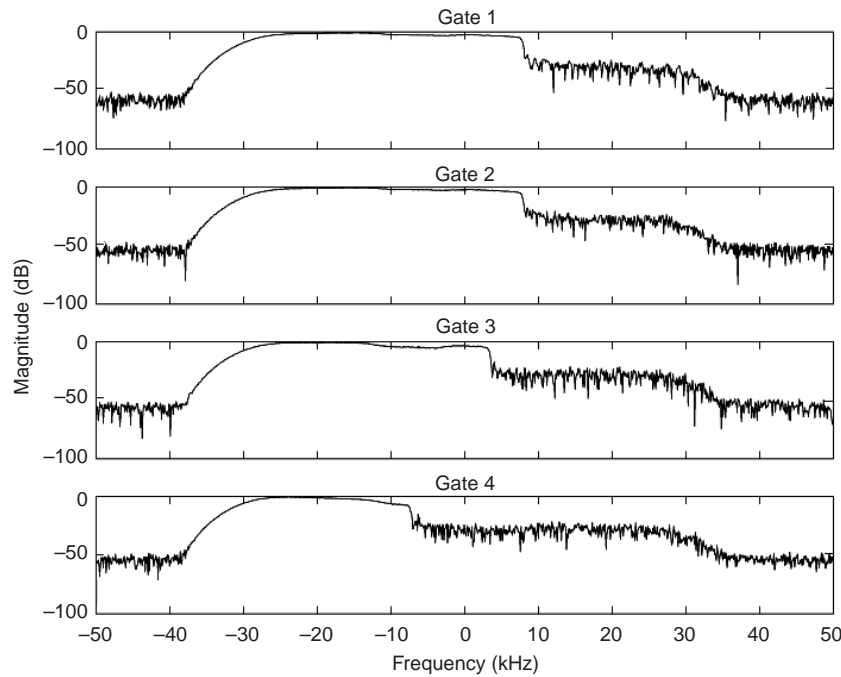


Figure 12. MRI navigator data.

EKG

Previous studies (e.g., Ref. 4) have suggested a correlation between the peak of the QRS complex of the EKG and respiration. Results of correlating the peak of the QRS complex and the R-R interval with the navigator data for 6 min are shown in Fig. 14, respectively. For the QRS peak, the data are nearly correlated, with some outlying data points corresponding to low EKG voltage. The discrepancy could be caused by induced voltages from the RF or gradients, either of which could be compensated for, or from the flow of blood ions in the strong static magnetic field of the scanner, i.e., the “magnetodynamic” effect. The artifact could be minimized using more EKG channels, as suggested by Fischer.⁵ The R-R interval measurements are poorly correlated.

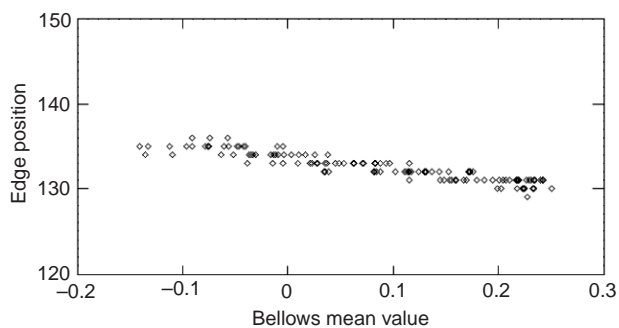


Figure 13. Correlation of stomach bellows and position of navigators (1 through 128).

Accelerometer

A plot of the data from the accelerometer on a normal volunteer outside the magnet is shown in Fig. 15. The low-frequency data are well correlated with the stomach bellows trace, and the high-frequency data appear a short time after the QRS peak. When the volunteer was placed inside the magnet, the high-frequency data obtained by simply filtering the signal were contaminated by the gradients. These data might be obtained more reliably by actively canceling the gradients. The low-frequency data are readily obtained, both inside and outside the magnet, using a low-pass filter.

Radar

The radar data are shown with respect to the other sensor data in Fig. 16a. This data set was derived before the MRI scanner was turned on. The radar signal shows an appropriate response when the bellows is in a transition period, i.e., changing at its highest rate. The heart motion can be seen on the radar signal as well. This could contain valuable information about the cardiac phase and position. Such information can also be seen on the accelerometer.

Figure 16b shows a similar plot after the MRI scanner was turned on, acquiring navigators on the abdomen. The spikes on the MRI gate data-trace show the precise timing as to when the gates were turned on. A significant amount of corruption due to the gradients is present on the accelerometer and radar signals. This

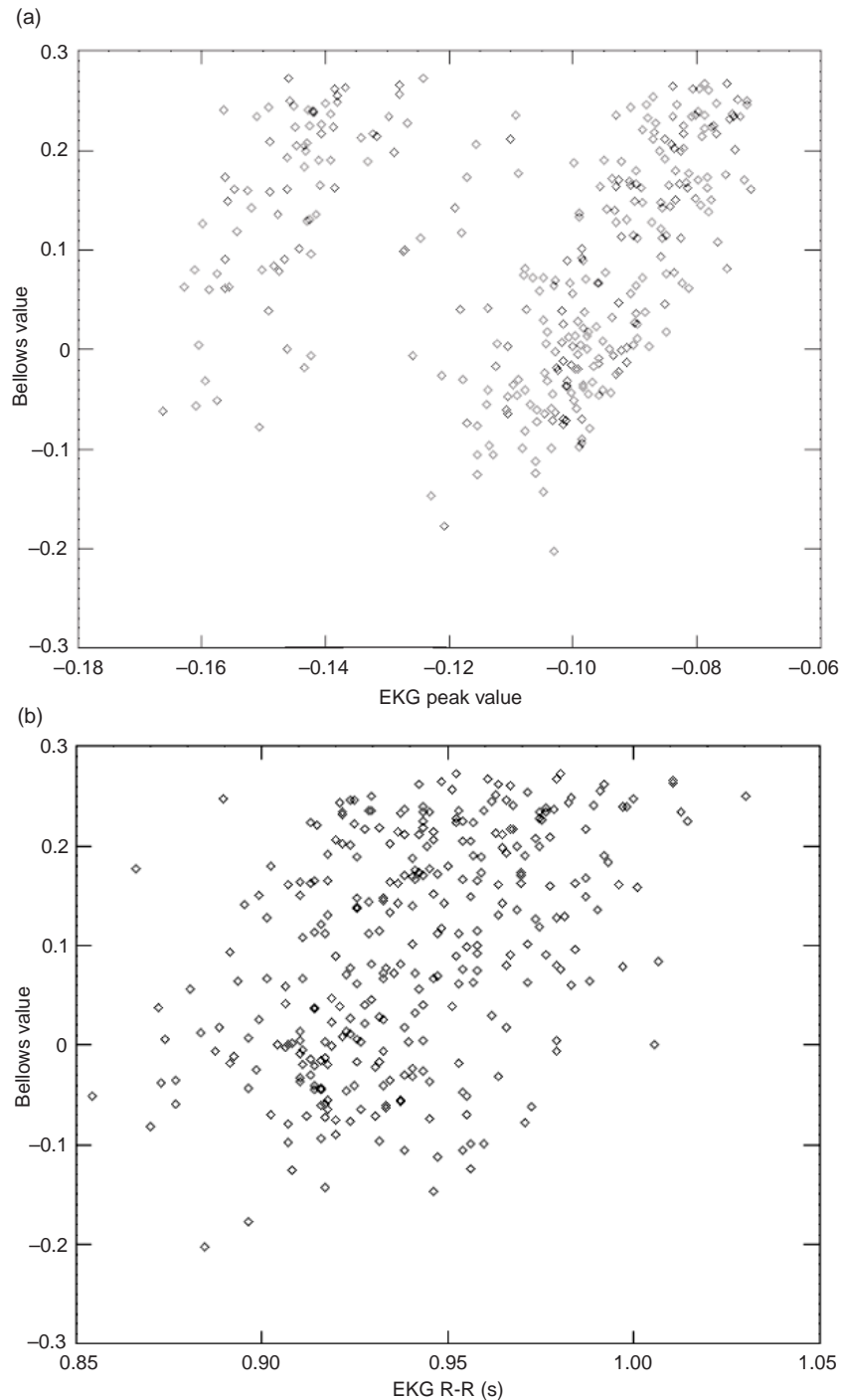


Figure 14. Correlation of stomach bellows with (a) peak of QRS complex and (b) EKG R-R interval for the first 319 EKGs.

corruption could be reduced using improved preamp and filtering circuitry.

CONCLUSION

Our results indicate that the stomach bellows data correlate well with diaphragm position in most volunteers. However, some volunteers required a bellows

placed on the chest to obtain a more accurate estimate. The peak of the QRS complex also appears to be correlated with the diaphragm location, but may be corrupted by the magnetodynamic effect. Sampling multiple EKG channels may remove the effect and lend insight into cardiac dynamics through the rotation of the cardiac vector. Accelerometer data may also yield information about the respiratory cycle and cardiac

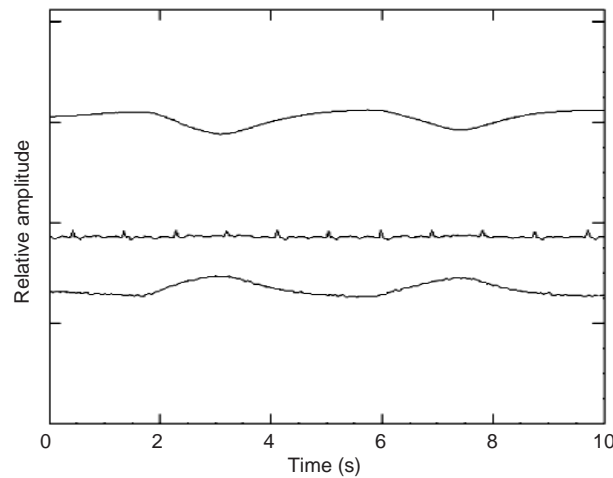
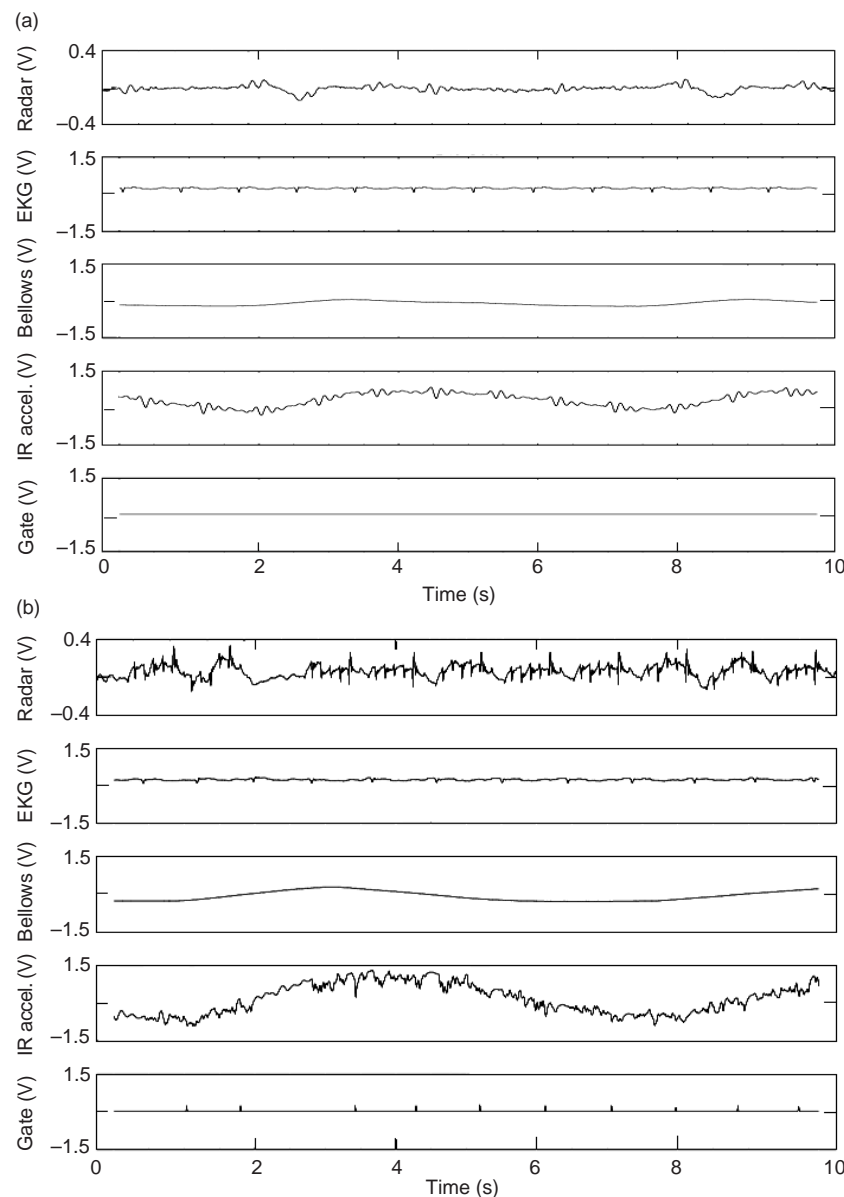


Figure 15. Plot of data from stomach bellows (top), EKG (center), and IR accelerometer (bottom).

dynamics, but these data were sometimes unreliable because of inadequate shielding. Correlations with the radar data are inconclusive because of excessive noise induced by the gradients. There is evidence that the radar signals would be useful in a gating system if the gradient noise could be controlled. More channels, either in the form of a chest bellows and multiple EKG leads or with an accelerometer, appear to be required for an accurate and reliable cardiac gating system.

FUTURE WORK

Several potential directions have come out of the investigations that APL has performed. First, the wireless telemetry could be expanded to include not only an accelerometer, but also several EKG leads. This would greatly reduce the wiring attached to the patient



and could enable more accurate cardiac gating. If wireless telemetry were successful, the technology could possibly be licensed to a small equipment manufacturer for production. Both the IR and RF wireless approaches have merit and should be pursued in parallel. Issues needing to be resolved on the RF wireless concern the poor signal coherence within the magnet. The IR wireless would require better shielding, and a new modulation technique would be needed to multiplex more information on the carrier. Because there is a gradient noise on the sensor signals, both approaches would benefit from an optical lead system from the wireless receiver to the patch panel. Figure 17 is a block diagram of a proposed multiple EKG and accelerometer transmit system. Such a system would have clear marketability.

The radar is another example of using RF within the Magnet Room, this time as an ancillary sensor. Two potential avenues exist for further development with respect to the radar. First, as an ancillary motion sensor, the current radar may not be able to distinguish

Figure 16. Plot of sensor data on a normal volunteer (a) before and (b) after the MRI scanner was turned on.

direction of motion, necessitating the use of an I/Q demodulator. Thus, it may be appropriate to add an I/Q demodulator or another radar that is direction sensitive. We have experimented with just such a radar, one that is relatively inexpensive and operates at 24 GHz, typical of automatic door opening systems. Logistics would still need to be worked out, since it is unknown whether this radar would have enough return power when being used from the same location as the police radar. One approach with this radar would be to use a nonferrous waveguide from outside the bore of the main magnet to within the magnet. Certainly there would be enough return power if it were pointing straight down on the patient, and it might become a more specific sensor than the other radar ≈ 4.6 m away from the main magnet. The waveguide and small door-opening radar exist at APL, where several experiments were conducted. Results showed that this radar could sense both respiratory and heart beat surface deflections on a person from a short distance. No attempt has been made, however, to incorporate this sensor with the others in close proximity to the MRI scanner.

The second avenue using the radar would be to examine longer wavelength systems, which would have more penetration than the radar systems we have been examining. The potential exists to combine both an MRI scanner with a crude radar imaging system. From previous work, a short pulse centered at about 1 GHz would have both bandwidth and penetration potential. We found that Lawrence Livermore National

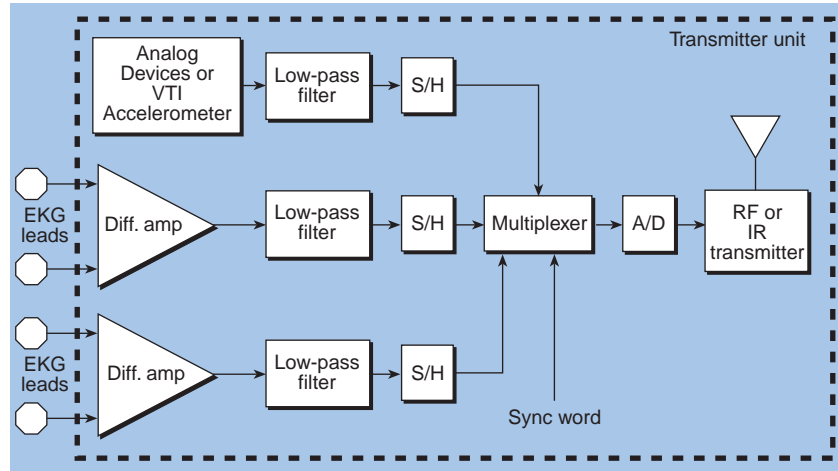


Figure 17. Block diagram of a modular, wireless accelerometer/multiple EKG.

Laboratories had developed a system called the Micro-powered Impulse Radar (MIR), a small, inexpensive, but still quite immature system. However, such a short-pulse or impulse radar system does have the potential to do ranging, and this could be important in determining interface positions within a person being scanned.

REFERENCES

- ¹Levanon, N., *Radar Principles*, John Wiley & Sons, New York (1988).
- ²Ramo, S., Whinnery, J., and vanDuzer, T., *Fields and Waves in Communication Electronics*, John Wiley & Sons, New York (1984).
- ³Stoy, R., Foster, K., and Schwan, H., "Dielectric Properties of Mammalian Tissues from 0.1 to 100 MHz: A Summary of Recent Data," *Phys. Med. Biol.* **37**, 501-513 (1982).
- ⁴Felbinger, J., and Boesch, C., "Amplitude Demodulation of the Electrocardiogram Signal (ECG) for Respiration Monitoring and Compensation During MR Examinations," *MRM* **38**, 129-136 (1997).
- ⁵Fischer, S., Wickline, S., and Lorentz, C., "Robust Real-Time R-Wave Detection Based on the Vector Cardiogram," *Proc. ISMRM* **6**, 742 (Apr 1998).

ACKNOWLEDGMENTS: We would like to thank Frank Marcote, Jim Hanson, and Allen Bric for their engineering support, Henry Kues and Lex Hughes for their radar help, and Robert Balaban for time on the scanner in the Laboratory of Cardiac Energetics.

THE AUTHORS



RUSSELL J. IANNUZZELLI received a B.S. in electrical engineering from Drexel University in 1982 and an M.A. in applied mathematics from the University of Maryland in 1987. He joined APL in 1982 and is a member of the Senior Professional Staff in the Air Defense Systems Department's Combat Systems Development Group. Mr. Iannuzzelli has been involved in signal processing analysis and real-time software implementations for over 15 years. He has worked on the Terrier Fire Control System, the Standard Missile Program, Noncooperative Target Recognition, the Norway Ocean Radar, and the Bistatic Vortex Detection Radar. Most recently, he has worked on several real-time implementations related to cardiac MRI. His e-mail address is russell.iannuzzelli@jhuapl.edu.



PATRICK N. MORGAN received a B.S. degree from Duke University in 1989, an M.S. degree from UCLA in 1991, and a Ph.D. from Stanford University in 1996, all in electrical engineering. At Stanford, he developed instrumentation for a low-cost MRI scanner while supported by a National Science Foundation Graduate Research Fellowship. During 1996–1998, as a member of the APL Senior Staff, Dr. Morgan worked to develop a real-time MRI system and an improved gating system for cardiac MRI. In 1998, he joined the Electrical Engineering Department at Texas A&M University as an Assistant Professor. His research interests include real-time MRI, prepolarized MRI, and optimal magnet design. His e-mail address is morgan@ee.tamu.edu.



BERNARD E. KLUGA is an Engineering Assistant with the Air Defense Systems Department's Combat Systems Development Group and has worked at APL since 1985. He has been involved with the development of the Terrier/Tartar "land-based test site" at APL, and has also worked on projects such as Captive Seeker, The Wake Vortex Experiment, Flare Genesis, CEC, and The Amateur Sky Survey (*Sky & Telescope*, Feb 98). Currently the president of the APL Astronomy Club, Mr. Kluga participates in the club's outreach learning program for the local school systems. He is a member of the American Astronomical Society and S.P.I.E. His e-mail address is bernard.kluga@jhuapl.edu.



MICHELLE M. ROCKWELL received her B.S.E.E. degree from the University of Maryland in 1994. She joined APL's Fleet Systems Department in 1996 and is currently a member of the Associate Professional Staff in the Air Defense Systems Department. In addition to the MRI gating project, Ms. Rockwell worked extensively on radar systems analyses for the Trilateral Frigate Cooperative (TFC) project. She is currently continuing her work in the TFC project and has recently joined in the DEXA project, which involves the design and construction of an X-ray densitometer to measure bone strength and density. Her e-mail address is michelle.rockwell@jhuapl.edu.